Article

Synthesis, Characterization, and Photocatalytic Properties of Sol-Gel Ce-TiO$_2$ Films

Lidija Ćurković [1,*], Debora Briševac [1], Davor Ljubas [1,*], Vilko Mandić [2] and Ivana Gabelica [1]

[1] Faculty of Mechanical Engineering and Naval Architecture, University of Zagreb, 10000 Zagreb, Croatia; debora.brisevac@fsb.unizg.hr (D.B.); ivana.gabelica@fsb.unizg.hr (I.G.)
[2] Faculty of Chemical Engineering and Technology, University of Zagreb, 10000 Zagreb, Croatia; vmandic@fkit.unizg.hr
[*] Correspondence: lidija.curkovic@fsb.unizg.hr (L.Ć.); davor.ljubas@fsb.unizg.hr (D.L.)

Abstract: In this study, nanostructured cerium-doped TiO$_2$ (Ce-TiO$_2$) films with the addition of different amounts of cerium (0.00, 0.08, 0.40, 0.80, 2.40, and 4.10 wt.%) were deposited on a borosilicate glass substrate by the flow coating sol-gel process. After flow coating, the deposited films were dried at a temperature of 100 °C for 1 h, followed by calcination at a temperature of 450 °C for 2 h. For the characterization of sol-gel TiO$_2$ films, the following analytic techniques were used: X-ray diffraction (XRD), differential thermal analysis (DTA), thermal gravimetry (TG), differential scanning calorimetry (DSC), diffuse reflectance spectroscopy (DRS), and energy dispersive X-ray spectroscopy (EDS). Sol-gel-derived Ce-TiO$_2$ films were used for photocatalytic degradation of ciprofloxacin (CIP). The influence of the amount of Ce in TiO$_2$ films, the duration of the photocatalytic decomposition, and the irradiation type (UV-A and simulated solar light) on the CIP degradation were monitored. Kinetics parameters (reaction kinetics constants and the half-life) of the CIP degradation, as well as photocatalytic degradation efficiency, were determined. The best photocatalytic activity was achieved by the TiO$_2$ film doped with 0.08 wt.% Ce, under both UV-A and solar irradiation. The immobilized catalyst was successfully reused for three cycles under solar light simulator radiation, with changes in photocatalytic efficiency below 3%.

Keywords: Ce-TiO$_2$; ciprofloxacin; photocatalysis; characterization

1. Introduction

Wastewater released into the environment can have an extremely harmful effect on the nature and well-being of living creatures. Research showed that the most significant amount of pharmaceuticals released into the environment came from wastewater treatment plants [1,2]. The primary sources of pollution are sewage collected from households, hospitals, etc. The result of wastewater discharge into the environment is the pollution of soil, surface and underground waters (rivers, lakes, seas), and drinking water [3,4]. In order to reduce or, at best, eliminate pollutants, numerous water and air purification techniques are being developed, such as chemical precipitation, filtration, electrodeposition, adsorption, membrane systems, etc. [5–7]. These conventional water treatment processes are no longer efficient enough for the degradation of complex substances such as pharmaceuticals, their metabolites, or transformation products [1,3]. Advanced oxidation processes (AOPs), especially heterogeneous photocatalysis, have shown their promising ability for degradation through the generation of hydroxyl radicals (OH·). These are able to react with the pollutants they come into contact with, serving as powerful oxidizing agents [8,9].

Numerous studies have confirmed that some photocatalysts, such as TiO$_2$, Fe$_2$O$_3$, WO$_3$, ZnO, CeO$_2$, CdS, ZnS, MoO$_3$, ZrO$_2$, and SnO$_2$, can be activated by light due to the favorable size of the energy gap and their electronic structure with a free conduction band and a filled valence band, and thus break down toxic organic substances in water

and air [5,10]. Photocatalysts can completely decompose harmful organic substances into simple compounds such as water, carbon dioxide, and corresponding mineral acids [6,11].

TiO_2 is recognized as an excellent photocatalyst, but due to its relatively high band gap energy of 3.2 eV for the anatase phase and 3.03 eV for the rutile phase, it can only be used when irradiated with UV radiation $\lambda < 387$ nm, which makes up only 3–5% of the total naturally occurring solar radiation [6,8,10–12]. In order to extend the photocatalytic activity of TiO_2 into the visible range of electromagnetic radiation, it is often doped with non-metals (N, S, C, H) [13,14], noble metals (Ag, Au, Pt) [15], transition metals (Ce, Fe) [16], modified with metal semiconductors, co-doped with metals and non-metals, etc. [8,10,16–18].

The sol-gel method for the preparation of nanostructured cerium-doped titania has shown promising results in shifting the photocatalytic activity of TiO_2 into the visible range of irradiation [8,12,19–22]. By increasing the concentration of cerium in TiO_2, the band gap of TiO_2 narrows. Consequently, TiO_2 begins to absorb visible light, shifting its absorption edge from UV to the visible spectrum up to 450 nm. This phenomenon is attributed to potential charge transfer between Ce $4f$ levels. The presence of cerium $4f$ levels is critical in suppressing the recombination of electron-hole pairs, thereby enhancing certain processes. However, excessive doping with cerium may introduce an abundance of recombination centers, thus diminishing the photodegradation capability of the material [8,12,23].

Methods that produce the photocatalyst in powder form are less often used because they require the removal of the photocatalyst from water by filtration and other separation processes, which adds another step during the processing and consumes time and resources. Today, the process of photocatalyst immobilization on various substrates has been increasingly used to avoid the complex removal step [7,24].

This research aimed to prepare nanosized sol-gel cerium-doped titania ceramic films (Ce-TiO_2) with varying amounts of cerium for use in photocatalytic oxidation experiments. The Ce-TiO_2 films were deposited on borosilicate glass substrates using the sol-gel flow coating method. Ciprofloxacin, a widely used antibiotic, served as a model pollutant for this study, and its photocatalytic degradation was measured using UV-Vis measurements.

2. Materials and Methods

2.1. Preparation of Ce-TiO_2 Films

Nanostructured Ce-TiO_2 films were deposited on a borosilicate glass substrate via the sol-gel process using the flow coating method. The substrates were borosilicate glass plates with 30 mm × 50 mm × 2 mm dimensions. Prior to deposition, the substrates were carefully cleaned following the procedure previously described in [25].

TiO_2 sols (colloidal solutions) with different amounts of cerium (Ce) were prepared by mixing the following analytical grade reagents: titanium(IV) isopropoxide (TIP, $Ti(OCH(CH_3)_2)_4$, 98%, Sigma-Aldrich, St. Louis, MO, USA) as the precursor, cerium(III) nitrate hexahydrate ($CeN_3O_9·6H_2O$, 99.5%, Thermo Fisher Scientific, Waltham, MA, USA) as the precursor, i-propyl alcohol (PrOH, C_3H_7OH, 99.9%, Gram-Mol, Zagreb, Croatia) as the solvent, acetylacetone (AcAc. $CH_3(CO)CH_2COCH_3$, 99%+, VWR International, Radnor, PA, USA) as the chelating agent and nitric acid (HN, HNO_3, 65%, Carlo Erba Reagents, Val-de-Reuil, France) as the catalyst. The molar ratio of these reactants in all colloidal solutions was TIP:PrOH:AcAc:HN = 1:35:0.63:0.015 [26,27].

Six sols (colloidal solutions) were prepared as follows:

- TiO_2 sol without the addition of cerium (0.00 wt.% of cerium)
- TiO_2 sol with the addition of 0.08 wt.% of cerium
- TiO_2 sol with the addition of 0.40 wt.% of cerium
- TiO_2 sol with the addition of 0.80 wt.% of cerium
- TiO_2 sol with the addition of 2.40 wt.% of cerium
- TiO_2 sol with the addition of 4.10 wt.% of cerium.

The colloidal solutions underwent vigorous stirring for 2 h, followed by 30 min of sonication. The prepared sols were deposited on borosilicate glass samples, dried at 100 °C for 1 h, and then heat-treated at 450 °C for 2 h with a heating rate of 3 °C min^{-1}.

The deposition process using the flow coating method was repeated three times for each colloidal solution. The flow chart for the preparation of Ce-TiO$_2$ films using the sol-gel flow coating method is presented in Figure 1.
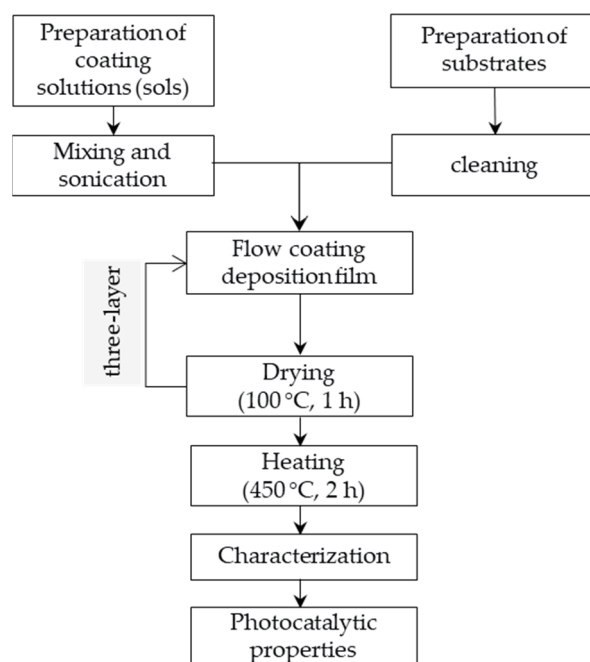
Figure 1. Flow chart for the preparation of Ce-TiO$_2$ films by the sol-gel flow coating method.

*2.2. Characterization of Sol-Gel Ce-TiO$_2$ Films*

Following the deposition of the sol-gel Ce-TiO$_2$ films onto a glass substrate, the remaining colloidal solutions were dried at 60 °C for 24 h to form dried gels. Portions of these dried gels were subjected to thermal gravimetry (TG) and differential scanning calorimetry (DSC). The remaining dried gels were calcined at a temperature of 450 °C for 2 h and prepared in powder form. Phase compositions, as well as parameters and volume of unit cell analysis, were conducted on Ce-TiO$_2$ powder samples using X-ray diffraction (XRD) on a D8 Advance Eco diffractometer (Bruker, Billerica, MA, USA) with CuKα radiation (l = 1.54055 Å) at 40 kV and 25 mA. The thermal characterization of the two samples (TiO$_2$ without the addition of cerium and TiO$_2$ with the addition of 0.08 wt.% of cerium) was carried out by means of simultaneous differential thermal and thermogravimetric analysis STA 409 (Netzsch, Selb, Germany). Diffuse reflectance spectra were recorded on 8° rotated powder samples on Perkin Elmer Lambda 1050+ with an InGaAs integrating sphere in the range from 250–1300 nm with a 2 nm resolution. The bandgap was then calculated from the onset of the remission function in dependence on the incident photon energy. Energy dispersive X-ray microscopy spectra were collected using the Nano Esprit 2 detector (Bruker, Billerica, MA, USA) at 10 kV and 15 mm working distance at 1000 magnification within the Vega Easyprobe 3 electron microscope (Tescan, Brno, Czech Republic).

2.3. Adsorption, Photolytic, and Photocatalytic Experiments

For experiments (dark adsorption, photolysis, and photocatalysis), analytical-grade ciprofloxacin (CIP, 98%, Acros Organics, Waltham, MA, USA) was used as the model organic micropollutant (OMP). Deionized water of ultrapure quality (electrical conductivity of 0.055 μS$\cdot$cm^{-1} at 25 °C) was used throughout the experiments. The solution of CIP (5 mg$\cdot$L^{-1}) was prepared by dissolving the appropriate amount of solid in ultrapure quality water. The photocatalytic activity of Ce-TiO$_2$ films with 0.00, 0.08, 0.40, 0.80, 2.40, and 4.10 wt.% of Ce was evaluated through the degradation of CIP using the following radiation

sources: UV-A lamp, model UVAHAND LED (Dr. Hönle AG, UV-Technologie, Gilching, Germany) (peak on 365 nm, 70 W), and solar light simulator (SLS) model SOL500 (Dr. Hönle AG, UV-Technologie, Gilching, Germany (430 W)).

The photocatalytic activity of pure TiO_2 and Ce-TiO_2 films with varying cerium concentrations was assessed in a borosilicate glass reactor measuring 95 mm in diameter, 55 mm in height, and with a volume of 250 mL. The solution was continuously stirred using a magnetic stirrer at 300 rpm. For each photocatalytic test, 4 glass plates coated with the photocatalytic film were placed at the bottom of the reactor, which contained 100 mL of the CIP solution (5 mg·L^{-1}). The reactor was irradiated from above with a lamp positioned 20 cm away. The magnetic stirrer was placed in the middle of the photoreactor, and the four glass plates were carefully arranged around the stirrer to prevent movement during mixing. The photoreactor was thermostated at 25 ± 0.2 °C. A schematic diagram of the side- and cross-section of the photoreactor is shown in Figure 2. After setting up, the lamp was turned on, and the suspension was irradiated for 2 h. Samples were taken from the reactor at specified intervals (0, 10, 20, 30, 45, 60, 90, 105, and 120 min), filtered through a 0.45 μm mixed cellulose ester membrane filter, and immediately analyzed using a UV-Vis spectrophotometer (HEWLETT PACKARD, Model HP 8430, Palo Alto, CA, USA) at the maximum absorption peak of CIP of 273 nm. Before irradiation, the solution was stirred in the dark for 15 min to ensure adsorption-desorption equilibrium, as determined by a prior adsorption test. Additionally, the photolytic activity of the CIP solution was tested under the same conditions but without the glass plates with photocatalytic films.

(**A**)   (**B**)
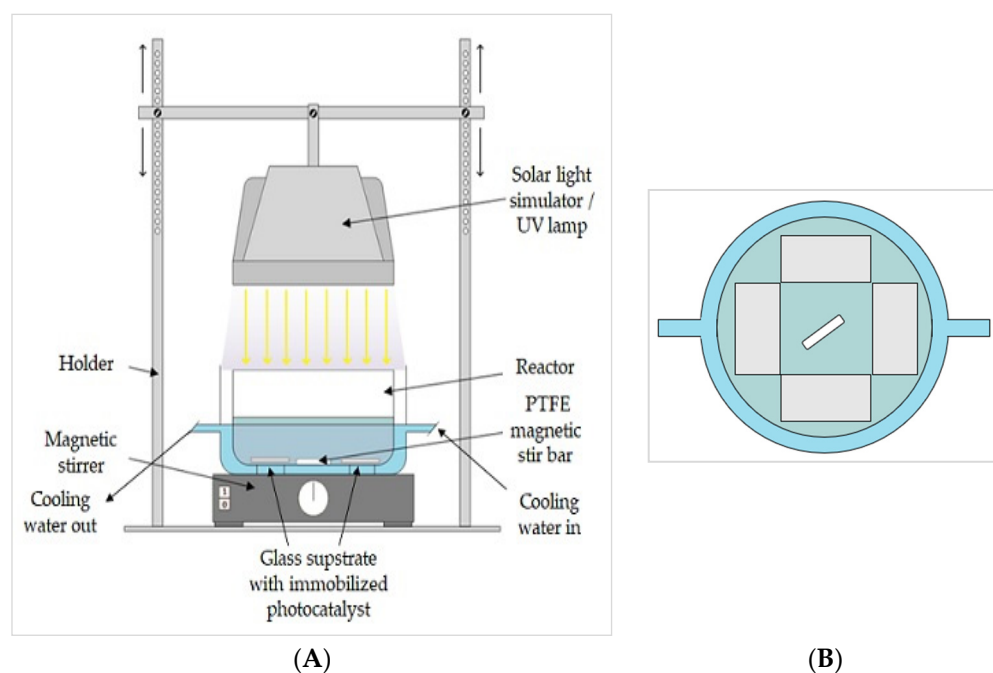
Figure 2. (**A**) Side- and (**B**) cross-section view of the photoreactor.

Pseudo-first-order kinetic models were employed to study the kinetics of the photocatalytic degradation of CIP using the prepared Ce-TiO_2 films. The linear form of the pseudo-first-order kinetic model is described by the following equation [28]:

$$-\ln \frac{A_t}{A_0} = k \cdot t \tag{1}$$

where k (min^{-1}) is the rate constant of the pseudo-first-order reaction of the photocatalytic decomposition of CIP, A_t is the absorbance of the CIP after irradiation at time t (min) during the photocatalytic process, and A_0 is the initial absorbance of the CIP.

The half-life ($t_{1/2}$, min) was calculated by the following equation [27]:

$$t_{1/2} = \frac{\ln 2}{k} \tag{2}$$

The photocatalytic degradation efficiency (η, %) of the degradation of CIP by prepared photocatalysts was calculated according to the following equation [29]:

$$\eta = \frac{A_0 - A_t}{A_0} \cdot 100\% \tag{3}$$

where A_0 is the initial absorbance of the CIP and A_t is the absorbance of the CIP at time t (min) during the photocatalytic process.

3. Results and Discussion

3.1. Characterization of Photocatalysts

The thermal analysis was carried out in order to determine the mass loss of samples of nanostructured TiO_2 powders and to monitor exothermic and endothermic reactions depending on the temperature. The analysis was carried out on two samples: TiO_2 powder without the addition of Ce and with the addition of 0.08 wt.% Ce. A comparison of the DSC/TG curves is shown in Figure 3. Changes were observed in the temperature interval from room temperature to 1000 °C. During the heating of both samples, there was an increase in their mass loss, which is characteristic of the thermal decomposition of amorphous gels.
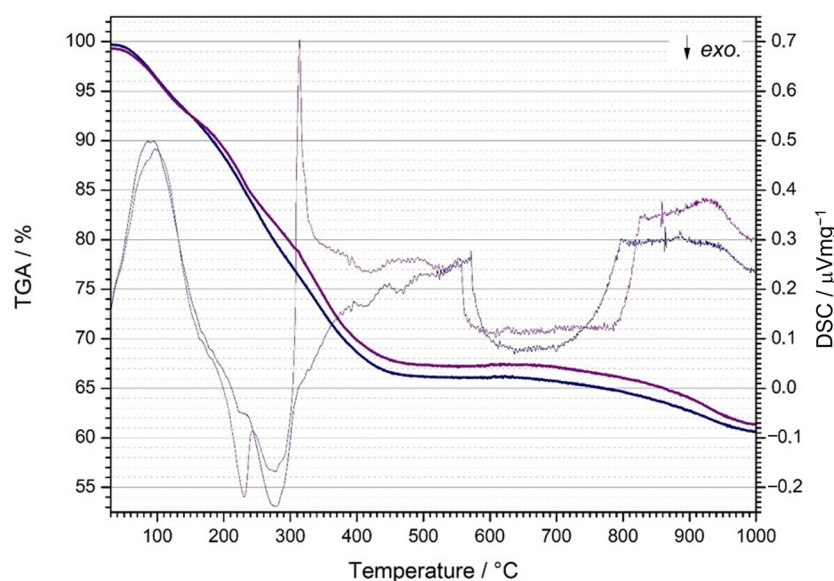

Figure 3. DSC/TG curves for TiO_2 without the addition of Ce (purple line) and TiO_2 with the addition of 0.08 wt.% Ce (blue line).

Two mass losses can be observed from the curves for both samples. In the area of lower temperatures, mass loss occurs due to the release of solvent and chemisorbed water, while around medium temperatures, decomposition and combustion of hydroxyl groups (OH^-) and organic phases present in the samples occur. The total mass loss of the TiO_2 sample without the addition of Ce is slightly higher than the mass loss of the TiO_2 sample with the addition of 0.08 wt.% Ce. When samples are heated, processes occur that are accompanied by the release (exothermic reactions) or the receipt of heat (endothermic reactions), i.e., a decrease or increase in the temperature of the samples in relation to the reference material, which is recorded as minima and maxima on the DSC curves. Both samples (TiO_2 and 0.08 wt.% Ce-TiO_2) have an endothermic minimum and an exothermic maximum. The

endothermic minimum is attributed to the desorption and release of substances from the gel, such as adsorbed water and alcohol. The exothermic maximums are attributed to the desorption of hydroxyl groups and other organic phases and the crystallization of the anatase phase of titanium dioxide. In the case of the 0.08 wt.% Ce-TiO$_2$ sample, a more complex course of thermal evolution with more pronounced multi-stage effects is visible, which is in accordance with the more complex composition of the precursor. In the case of the doped sample (0.08 wt.% Ce-TiO$_2$), anatase crystallization is shifted towards higher temperatures. In conclusion, the samples do not differ in the early stage of solvent loss, but undoped samples underwent more abrupt multistage exothermic events around 300 °C. The composition probably allowed for more significant auto-combustion behavior during heating. Notably, above 450 °C, the mass loss remains relatively constant (slightly less for the undoped sample), meaning the volatiles were removed. Only above 800 °C, the carbon remains burned off, resulting in additional slight mass loss.

XRD results point to the crystallization of TiO$_2$ predominately in the anatase structure. However, traces of rutile structure have been observed (Figure 4). Results of the XRD analysis of TiO$_2$ samples with different amounts (wt.%) of Ce (0.00, 0.08, 0.40, 0.80, 2.40, and 4.10) are presented in Figure 4. The obtained results showed that 0.08 wt.% Ce is easily incorporated into the TiO$_2$ lattice. Figure 4 shows that with a further increase in Ce amount, the rutile phase is absent, and Ce incorporation into the TiO$_2$ lattice significantly reduces. The crystallite size decreases linearly with increasing Ce content, from 45.8 nm (pure TiO$_2$) to 11.2 nm (TiO$_2$ with 4.1 wt.% of Ce). In the samples with 2.40 wt.% Ce-TiO$_2$ and 4.10 wt.% Ce-TiO$_2$, there are barely any traces of the cerium oxide phase.
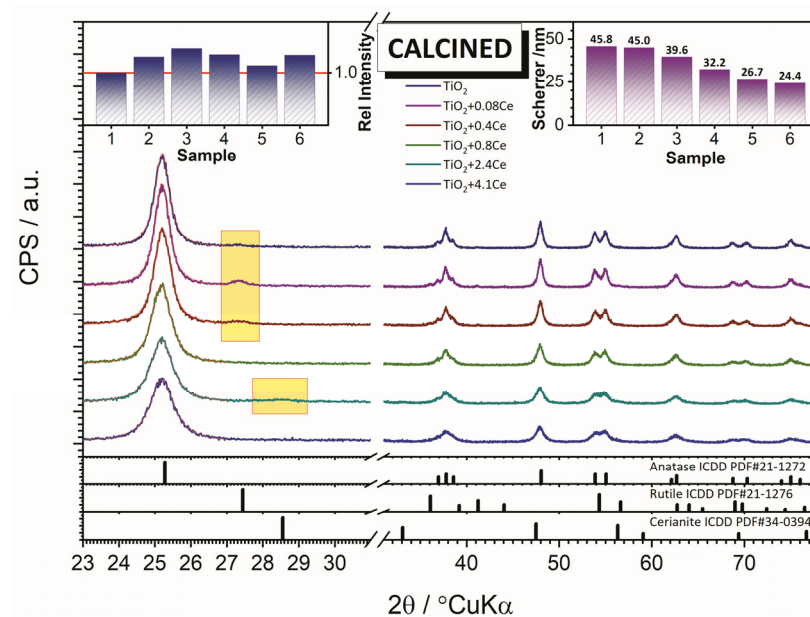
Figure 4. X-ray diffraction patterns and crystallite size TiO$_2$ samples with different amounts (wt.%) of Ce: 0.00, 0.08, 0.40, 0.80, 2.40, and 4.10.

The amount of incorporated Ce in the TiO$_2$ unit cell depends on the difference in the crystal radius of Ce^{4+} and Ti^{4+}. From the values of the parameters and the volume of the unit cell (Figure 5), it can be seen that smaller amounts of cerium (up to 0.08 wt.%) can be easily incorporated into the unit cell of anatase, while doping with Ce in amounts greater than 0.08 wt.% again leads to a decrease in parameter values and volume, which is a consequence of the difficulty of incorporating Ce^{4+} ions into the anatase unit cell. The radius of Ce^{4+} ions (0.092 nm) is much larger than the radius of Ti^{4+} ions (0.065 nm), so it is to be expected that a minimal amount of Ce^{4+} can be incorporated into the TiO$_2$ lattice and that an increase in the amount of Ce will result in the crystallization of additional separated phases of cerium oxide [24]. This behavior of the system is in accordance with the

qualitative diffraction analysis. Namely, the dopant cerium is introduced in the wet stage of the synthesis, which enables a homogeneous pre-crystalline network. Due to the proximity of the constituent elements, a lower treatment temperature is required to form the TiO_2 crystalline lattice, and it was easier for Ce to enter that lattice. Therefore, on behalf of the wet chemistry synthesis, we maximized the solubility ratio of Ce in TiO_2. Solubility, in this case, means substitutional doping, i.e., Ce takes the place of the Ti in the TiO_2 lattice, but this is not metallic Ce; it is ionic, i.e., the crystalline radius is relevant. Therefore, the crystal radii and charge determine solubility levels. Namely, the TiO_2 crystal lattice will easily form solid solutions with lower-level Ce doping, i.e., Ce-doped TiO_2 will be a single-phase system resembling TiO_2 with slightly changed properties. Increasing the doping will affect the unit cell in terms of expansion or contraction (due to the entrance of larger or smaller ions), and that is reliably evidenced through the change of the unit cell parameters (via XRD measurements). Once the doping maxima are reached, the excess Ce will not be able to penetrate the TiO_2 unit cell anymore and will remain "outside" of the TiO_2 and react with the ambient environment (oxidize) and from TiO_2 (or other Ce-based oxides) in the form of separate phases. We call that phase separation. When we see the presence of Ce-oxides, we know that we have surpassed the maximum suitable doping levels for the system. If we aimed for a single phase, then the phase separation is unwanted. However, such phase-separated composites can sometimes facilitate synergistic performance, especially for photocatalytic purposes.
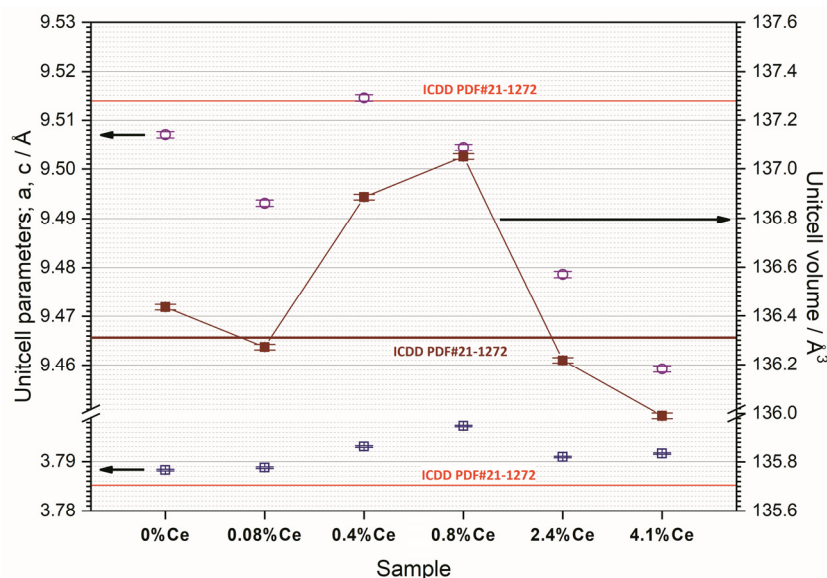
Figure 5. Parameters and volume of unit cells of TiO_2 samples with different amounts (wt.%) of Ce: 0.00, 0.08, 0.40, 0.80, 2.40, and 4.10.

The DRS was performed using Kubelka–Munk F(R) and Tauc plots, and the respective bandgaps were calculated. In the reflectance spectra, it can be seen that the utilization of visible light increases with increasing ceria content. As expected, on behalf of the substitutional doping, the material changed the crystal lattice, changing the respective energy levels and consequently affecting the bandgap value. Since this is most likely p-type doping, ceria introduces new acceptor levels near the valence band in the crystal lattice of the material. This acceptor energy level makes electron excitation easier by providing an intermediate metastable energy level at which electrons of low energy can exist without recombining, ultimately reducing the bandgap energy of the material. However, since electrons go through a series of energy levels by excitation from lower photon energies, this reflects on the remission function as a slow and steady transition from ground to excited state as opposed to the sharp increase in absorption, as seen for pristine TiO_2. Since these transitions are not sharp, the calculation of the bandgap via Kubelka–Munk should not be

taken for granted. The lower the slope of the function, the greater the error. Most likely, the real bandgap values for the samples with 2.4 and 4.1 wt.% Ce are definitely above 2.5 eV. Results are given in Figure 6A,B.
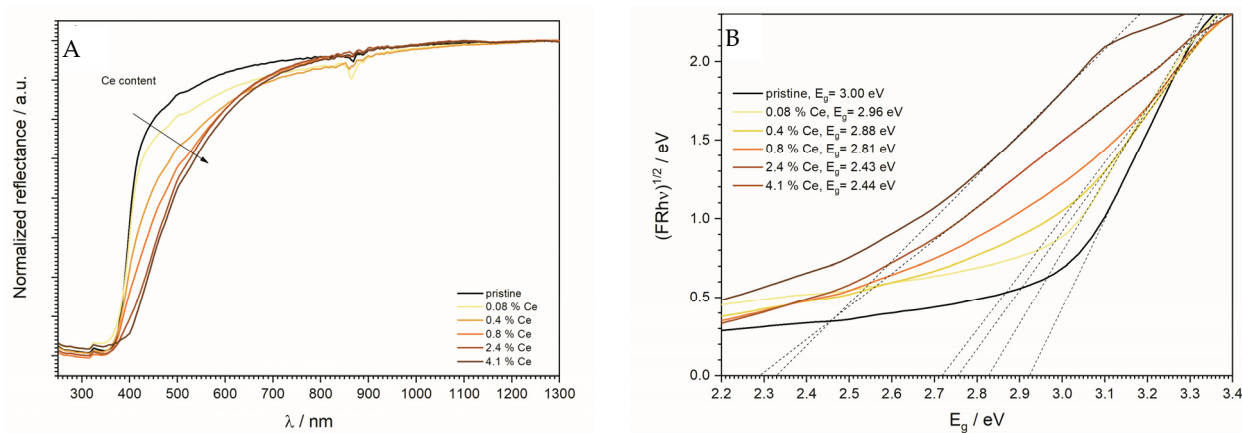
Figure 6. (**A**) DRS Kubelka–Munk spectra for TiO_2 and all Ce-doped samples, and (**B**) Tauc's plots with bandgap energy values.

The change of the unit cell parameters is the most reliable indicator with regard to the positioning of the Ce doping in terms of the interstitial or substitutional type of doping. Energy dispersive spectroscopy (EDS) was used to identify the elements (Ti, Ce, and O) present in the samples. It is well known that the values obtained by EDS are not to the point exact, but they fairly serve a point in terms of confirming the ratios of elements (Figure 7).
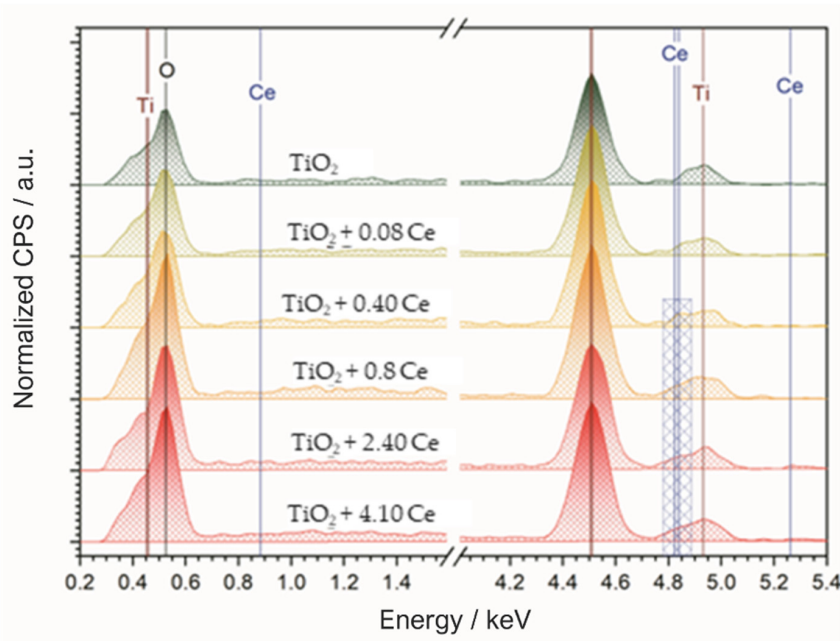

Figure 7. Energy-dispersive X-ray (EDS) spectrum of the TiO_2 and all Ce-doped samples.

3.2. Photocatalytic Properties of TiO_2 and Ce-TiO_2 Films

The photoactivity of the TiO_2 films with the different amounts (wt.%) of Ce (0.00, 0.08, 0.40, 0.80, 2.40, and 4.10) was evaluated through the degradation of CIP aqueous solution (5 mg·L^{-1}) under UVA light (Figure 8A) and a solar light simulator (Figure 8B). Figure 8 shows the kinetics of photolytic and photocatalytic degradation of CIP, i.e., the dependence of the change in the relative absorbance value (A/A_0) versus time (t, min). Before the photocatalytic test, dark adsorption (D. A.) was performed (Figure 8A,B). The

initial pH of the CIP solution was in the range of 6.3–6.5; after the experiments (adsorption, photolysis, and photocatalysis), the pH values were kept the same. The dark adsorption of ciprofloxacin on TiO_2 and $Ce-TiO_2$ films was negligible. The best photocatalytic properties were achieved by TiO_2 film doped with 0.08 wt.% of Ce by UV-A (365 nm) and solar light simulator radiation. For all $Ce-TO_2$ films, better photocatalytic properties were achieved by solar light simulator radiation compared to UV-A (365 nm) radiation.
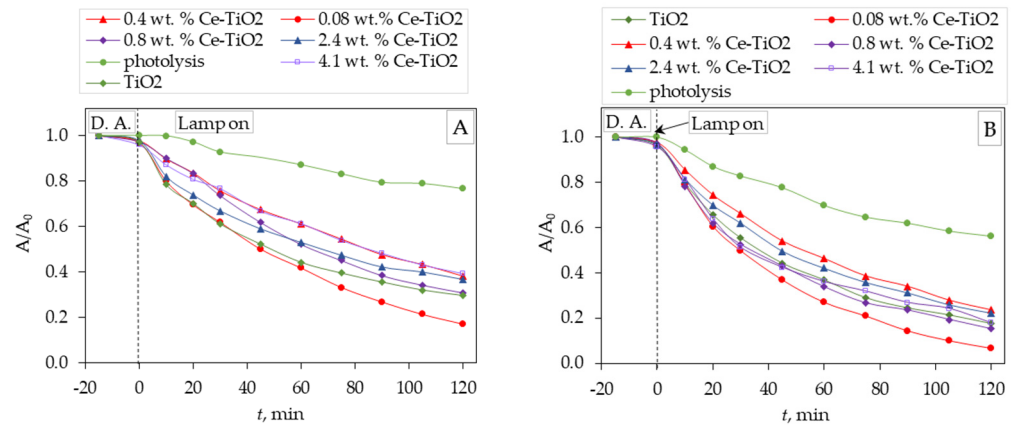
Figure 8. Photolytic and photocatalytic degradation of CIP under (**A**) UV-A (365 nm) and (**B**) solar light simulator radiation by sol-gel $Ce-TiO_2$ films as a function of irradiation time, γ_0 (CIP) = 5 mg·L^{-1}.

The photolytic and photocatalytic data are described using the pseudo-first-order model. The pseudo-first-order rate constant k from Equation (1) is evaluated through the linear regression of $-\ln(A/A_0)$ versus *t* (Figure 9). The pseudo-first-order model describes a process in which the degradation rate is mainly affected by changes in pollutant concentration [30].
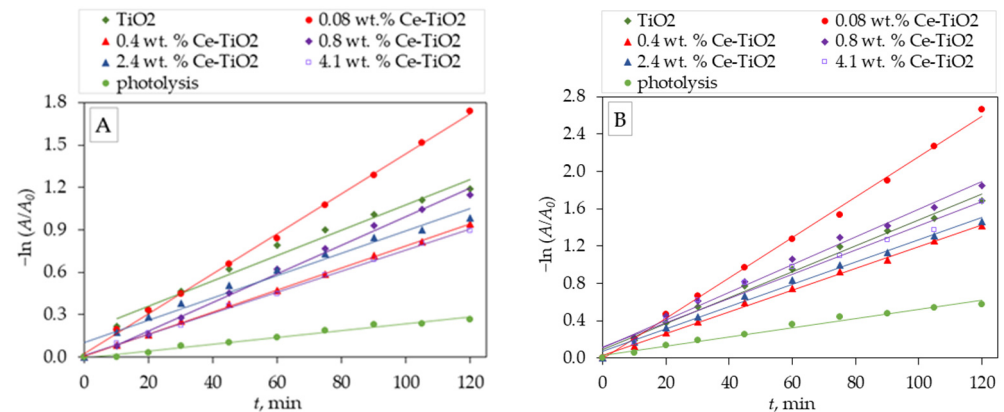
Figure 9. Linear transformation of $-\ln(A/A_0)$ versus *t* of photolytic and photocatalytic degradation of CIP under (**A**) UV-A (365 nm) and (**B**) solar light simulator radiation by sol-gel $Ce-TiO_2$ films, γ_0 (CIP) = 5 mg·L^{-1}.
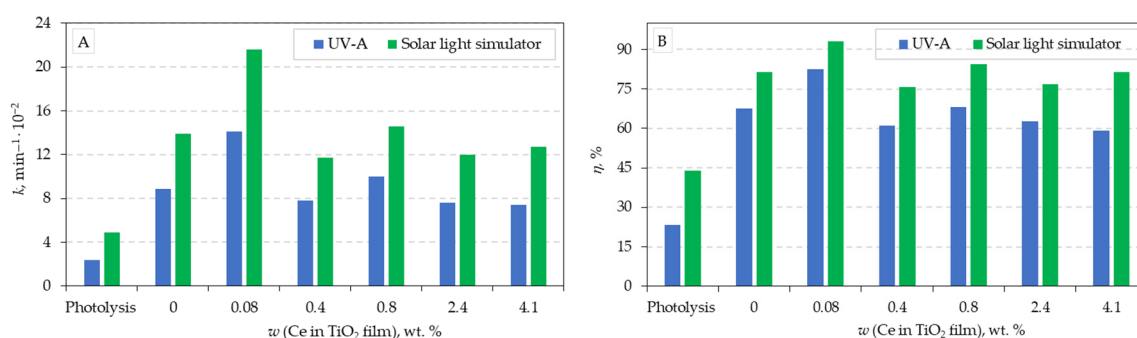
The kinetic constant for the pseudo-first-order is obtained from the slope of the plot of $-\ln(A/A_0)$ versus the irradiation time (Figure 9).

Calculated values of the pseudo-first-order (k, min^{-1}), the half-life ($t_{1/2}$, min), and the removal efficiencies of $Ce-TiO_2$ films are listed in Table 1. The pseudo-first-order model shows that under UV and solar light, the correlation coefficient (R^2) in all cases has a value above 0.98, indicating that the pseudo-first model describes both experimental degradation processes (photocatalytic and photolytic) well. A comparison of the obtained values of pseudo-first-order (k, min^{-1}) and removal efficiencies (η, %) for all experimental

conditions is presented in Figure 10A and 10B, respectively. From the photocatalytic tests, it can be seen that the TiO_2 film with the least addition of Ce (0.08 wt.%) has the highest photocatalytic efficiency and the highest CIP degradation rate constant for both radiation sources (Figure 10 and Table 1). By comparing the photocatalytic activity of the same films with both radiation sources, it can be observed that a higher photocatalytic efficiency and a higher degradation rate constant were achieved by applying solar light simulator radiation.

Table 1. The values of pseudo-first-order reaction rate constants (k, min^{-1}) and half-life times ($t_{1/2}$, min), along with the corresponding correlation coefficients (R^2) and removal efficiency of photocatalytic degradation of ciprofloxacin (γ_0 = 5 mg L^{-1}) by TiO_2 films with different amounts of Ce, under UV-A and SOLAR radiation, at a temperature of 25 °C.

Film	UV-A				Solar Light Simulator			
	$k \times 10^{-3}$, min^{-1}	$t_{1/2}$, min	R^2	η, %	$k \times 10^{-3}$, min^{-1}	$t_{1/2}$, min	R^2	η, %
Photolysis (without film)	2.4	288.81	0.9840	23.35	4.9	141.46	0.9835	43.88
0 wt.% Ce-TiO$_2$	8.9	77.88	0.9815	67.53	13.9	49.87	0.9907	81.54
0.08 wt.% Ce-TiO$_2$	14.1	49.16	0.9989	82.38	21.6	32.09	0.9977	93.04
0.40 wt.% Ce-TiO$_2$	7.8	88.87	0.9991	61.03	11.7	59.24	0.9980	75.79
0.80 wt.% Ce-TiO$_2$	10.0	68.63	0.9945	68.22	14.6	47.48	0.9934	84.28
2.40 wt.% Ce-TiO$_2$	7.6	91.20	0.9863	62.58	12.0	57.76	0.9938	76.92
4.10 wt.% Ce-TiO$_2$	7.4	93.67	0.9990	59.12	12.7	54.58	0.9810	81.32

Figure 10. Comparison of the values of (**A**) pseudo-first-order kinetic constants and (**B**) degradation efficiency of photolytic and photocatalytic degradation of CIP under UV-A (365 nm) and solar light simulator radiation by sol-gel Ce-TiO$_2$ films, γ_0 (CIP) = 5 mg·L^{-1}.

Martins et al. prepared an Au/TiO_2 nanocomposite (Au loading ranging from 0.025 to 0.5 wt.%) for photocatalytic degradation of CIP (5 mg·L^{-1}) under UV and simulated visible light. Reaction rate constants varied from 0.047 to 0.131 min^{-1} for different Au loadings over 30 min of UV irradiation, while apparent reaction rates over 180 min of visible light irradiation varied from 0.073 to 0.242 min^{-1} for different Au loadings [31].

To overcome the separation process of the photocatalyst, Hassani et al. employed the immobilization of TiO_2 onto montmorillonite for the degradation of 20 mg·L^{-1} ciprofloxacin. In contrast to suspended TiO_2, which degraded only 57% (with a rate constant of 0.0063 min^{-1}), immobilized TiO_2 exhibited accelerated degradation (0.0069 min^{-1}) and achieved up to 62% degradation within 2 h [32].

Malakootian et al. also immobilized TiO_2 nanoparticles on a glass plate for photocatalytic degradation of CIP (5 mg·L^{-1}) under UV light. The reaction rate constant was 0.0193 min^{-1}, and removal efficiency was around 60% after 60 min of irradiation [33].

Different light sources as well as metal and non-metal doping of TiO_2 were widely investigated by numerous scientists for the degradation of ciprofloxacin. Their results are summarized by Imam et al. [34].

3.3. Reusability and Stability of the Immobilized Photocatalysts on the Glass Substrate

Immobilization of the photocatalyst on a suitable support is essential for practical application in the water treatment process. The reusability and stability of immobilized photocatalysts are important for practical application. Therefore, the immobilized catalysts were tested for confirmation of reusability and stability by repeating the degradation process three times for all films under solar light simulator radiation. The obtained results are presented in Figure 11.
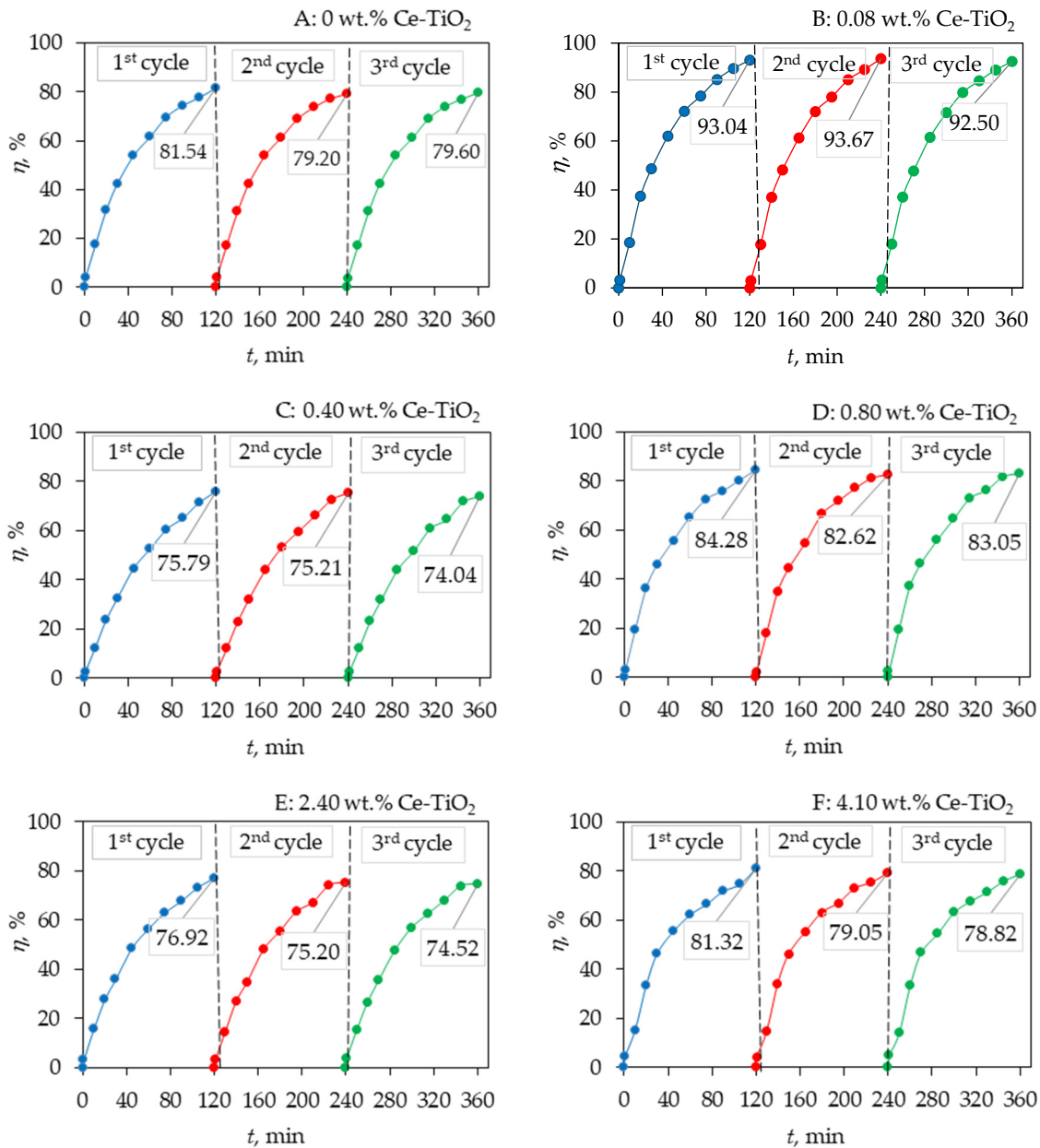
Figure 11. Reusability efficiency (η, %) of the sol-gel Ce-TiO$_2$ films for three consecutive cycles under solar light simulator radiation for TiO$_2$ film with different amounts of Ce: (**A**) 0.00 wt.%, (**B**) 0.08 wt.%, (**C**) 0.40 wt.%, (**D**) 0.80 wt.%, (**E**) 2.40 wt.%, and (**F**) 4.10 wt.%.

As shown in Figure 11, after three repetition cycles, the photodegradation efficiency of CIP did not show significant changes. The changes were below 3%, which indicated that all immobilized photocatalysts have good stability. Between each cycle, the glass substrate with photocatalyst film was removed from the reactor, washed, and dried. For

other conditions (adsorption, photolysis, and photocatalysis under UV light), repetition tests (three tests) were performed to ensure reproducibility; the changes were below 3%.

4. Conclusions

This paper presents the results of the photolytic and photodegradation processes of a diazo CIP aqueous solution in the presence of Ce-TiO$_2$ films under UV-A (365 nm) and solar light simulator radiation. Six sol-gel TiO$_2$ films with different amounts of Ce (0.00, 0.08, 0.40, 0.80, 2.40, and 4.10 wt.%) were deposited on a glass substrate by a flow coating method.

The crystallite size as well as phase composition are changed by changing the amount of Ce in TiO$_2$ samples.

These results indicate that the photocatalytic properties of sol-gel TiO$_2$ films depend on the amount of added Ce.

The mechanisms of photocatalytic oxidation of the CIP by sol-gel TiO$_2$ films were described by a pseudo-first-order kinetic model. The obtained values of the determination coefficient R^2 (all values were above 0.98) indicate that the pseudo-first-order rate is suitable for describing the photodegradation process of CIP photocatalytic degradation with sol-gel Ce-TiO$_2$ films as the photocatalyst.

It was found that sol-gel TiO$_2$ film with the least addition of Ce (0.08 wt.%) has the highest photocatalytic efficiency and the highest CIP degradation rate constant for both radiation sources. Comparing the photocatalytic activity of the same films with both radiation sources, it can be concluded that applying solar light simulator radiation achieved a higher photocatalytic efficiency and a higher degradation rate constant. This could be used for further use of natural solar radiation in real wastewater treatment plants for the degradation of other OMPs present in the water sample.

Author Contributions: Conceptualization, L.Ć., D.L. and D.B.; methodology, L.Ć., D.L. and D.B.; software, L.Ć., D.L., V.M., D.B. and I.G.; validation, L.Ć., D.L., V.M., D.B. and I.G.; formal analysis, D.B., V.M. and I.G.; investigation, D.B.; resources, L.Ć., D.L. and V.M.; data curation, L.Ć., D.L., V.M., D.B. and I.G.; writing—original draft preparation, L.Ć., D.B., D.L. and I.G.; writing—review and editing, L.Ć., D.L., V.M., D.B. and I.G.; visualization, L.Ć., D.L., V.M., D.B. and I.G.; supervision, D.L. and L.Ć.; project administration, L.Ć. and D.L.; funding acquisition, L.Ć. and D.L. All authors have read and agreed to the published version of the manuscript.

Data Availability Statement: The data presented in this study are available upon reasonable request from the corresponding author.

Conflicts of Interest: The authors declare no conflicts of interest.

References

1. Ganthavee, V.; Trzcinski, A.P. Removal of pharmaceutically active compounds from wastewater using adsorption coupled with electrochemical oxidation technology: A critical review. *J. Ind. Eng. Chem.* **2023**, *126*, 20–35. [CrossRef]
2. Kulišťáková, A. Removal of pharmaceutical micropollutants from real wastewater matrices by means of photochemical advanced oxidation processes—A review. *J. Water Proc. Eng.* **2023**, *53*, 103727. [CrossRef]
3. Santos, L.H.M.L.M.; Araújo, A.N.; Fachini, A.; Pena, A.; Delerue-Matos, C.; Montenegro, M.C.B.S.M. Ecotoxicological aspects related to the presence of pharmaceuticals in the aquatic environment. *J. Hazard. Mater.* **2010**, *175*, 45–95. [CrossRef] [PubMed]
4. Patel, M.; Kumar, R.; Kishor, K.; Mlsna, T.; Pittman, C.U.; Mohan, D. Pharmaceuticals of Emerging Concern in Aquatic Systems: Chemistry, Occurrence, Effects, and Removal Methods. *Chem. Rev.* **2019**, *119*, 3510–3673. [CrossRef]
5. Etacheri, V.; Di Valentin, C.; Schneider, J.; Bahnemann, D.; Pillai, S.C. Visible-light activation of TiO$_2$ photocatalysts: Advances in theory and experiments. *J. Photochem. Photobiol. C* **2015**, *25*, 1–29. [CrossRef]
6. Teh, C.M.; Mohamed, A.R. Roles of titanium dioxide and ion-doped titanium dioxide on photocatalytic degradation of organic pollutants (phenolic compounds and dyes) in aqueous solutions: A review. *J. Alloys Compd.* **2011**, *509*, 1648–1660. [CrossRef]
7. Kryuchkova, M.; Batasheva, S.; Akhatova, F.; Babaev, V.; Buzyurova, D.; Vikulina, A.; Volodkin, D.; Fakhrullin, R.; Rozhina, E. Pharmaceuticals Removal by Adsorption with Montmorillonite Nanoclay. *Int. J. Mol. Sci.* **2021**, *22*, 9670. [CrossRef]
8. Cerrato, E.; Gaggero, E.; Calza, P.; Paganini, M.C. The role of Cerium, Europium and Erbium doped TiO$_2$ photocatalysts in water treatment: A mini-review. *Chem. Eng. J.* **2022**, *10*, 100268. [CrossRef]

9.   Shan, A.Y.; Ghazi, T.I.M.; Rashid, S.A. Immobilisation of titanium dioxide onto supporting materials in heterogeneous photocatalysis: A review. *Appl. Catal. A-Gen.* **2010**, *389*, 1–8. [CrossRef]

10.   Umar, K.; Aris, A.; Ahmad, H.; Parveen, T.; Jaafar, J.; Majid, Z.A.; Reddy, A.V.B.; Talib, J. Synthesis of visible light active doped TiO$_2$ for the degradation of organic pollutants—Methylene blue and glyphosate. *J. Anal. Sci. Technol.* **2016**, *7*, 29. [CrossRef]

11.   Lan, Y.; Lu, Y.; Ren, Z. Mini review on photocatalysis of titanium dioxide nanoparticles and their solar applications. *Nano Energy* **2013**, *2*, 1031–1045. [CrossRef]

12.   Marami, M.B.; Farahmandjou, M. Water-Based Sol–Gel Synthesis of Ce-Doped TiO$_2$ Nanoparticles. *J. Electron. Mater.* **2019**, *48*, 4740–4747. [CrossRef]

13.   Li, G.; Zou, B.; Feng, S.; Shi, H.; Liao, K.; Wang, Y.; Wang, W.; Zhang, G. Synthesis of N-Doped TiO$_2$ with good photocatalytic property. *Phys. B Condens. Matter* **2020**, *588*, 412184. [CrossRef]

14.   Yan, J.; Zhao, J.; Hao, L.; Hu, Y.; Liu, T.; Guan, S.; Zhao, Q.; Zhu, Z.; Lu, Y. Low-temperature S-doping on N-doped TiO$_2$ films and remarkable enhancement on visible-light performance. *Mater. Res. Bull.* **2019**, *120*, 110594. [CrossRef]

15.   Mahmoudian-Boroujerd, L.; Karimi-Jashni, A.; Hosseini, S.N.; Paryan, M. Optimization of rDNA degradation in recombinant Hepatitis B vaccine production plant wastewater using visible light excited Ag-doped TiO$_2$ nanophotocatalyst. *Process Saf. Environ. Prot.* **2019**, *122*, 328–338. [CrossRef]

16.   Kayani, Z.N.; Maria; Riaz, S.; Naseem, S. Magnetic and antibacterial studies of sol-gel dip coated Ce doped TiO$_2$ thin films: Influence of Ce contents. *Ceram. Int.* **2020**, *46*, 381–390. [CrossRef]

17.   Contreras-García, M.E.; García-Benjume, M.L.; Macías-Andrés, V.I.; Barajas-Ledesma, E.; Medina-Flores, A.; Espitia-Cabrera, M.I. Synergic effect of the TiO$_2$-CeO$_2$ nanoconjugate system on the band-gap for visible light photocatalysis. *Mater. Sci. Eng. B* **2014**, *183*, 78–85. [CrossRef]

18.   Abdullah, H.; Khan, M.R.; Pudukudy, M.; Yaakob, Z.; Ismail, N.A. CeO$_2$-TiO$_2$ as a visible light active catalyst for the photoreduction of CO$_2$ to methanol. *J. Rare Earths* **2015**, *33*, 1155–1161. [CrossRef]

19.   Sun, P.; Liu, L.; Cui, S.C.; Liu, J.G. Synthesis, Characterization of Ce-doped TiO$_2$ Nanotubes with High Visible Light Photocatalytic Activity. *Catal. Lett.* **2014**, *144*, 2107–2113. [CrossRef]

20.   Choudhury, B.; Borah, B.; Choudhury, A. Extending Photocatalytic Activity of TiO$_2$ Nanoparticles to Visible Region of Illumination by Doping of Cerium. *Photochem. Photobiol.* **2012**, *88*, 257–264. [CrossRef]

21.   Chen, F.; Ho, P.; Ran, R.; Chen, W.; Si, Z.; Wu, X.; Weng, D.; Huang, Z.; Lee, C. Synergistic effect of CeO$_2$ modified TiO$_2$ photocatalyst on the enhancement of visible light photocatalytic performance. *J. Alloys Compd.* **2017**, *714*, 560–566. [CrossRef]

22.   Shaari, N.; Tan, S.H.; Mohamed, A.R. Synthesis and characterization of CNT/Ce-TiO$_2$ nanocomposite for phenol degradation. *J. Rare Earths* **2012**, *30*, 651–658. [CrossRef]

23.   Lee, J.Y.; Choi, J.H. Sonochemical Synthesis of Ce-doped TiO$_2$ Nanostructure: A Visible-Light-Driven Photocatalyst for Degradation of Toluene and O-Xylene. *Materials* **2019**, *12*, 1265. [CrossRef]

24.   Cao, X.P.; Li, D.; Jing, W.H.; Xing, W.H.; Fan, Y.Q. Synthesis of visible-light responsive C, N and Ce co-doped TiO$_2$ mesoporous membranes via weak alkaline sol–gel process. *J. Mater. Chem.* **2012**, *22*, 15309–15315. [CrossRef]

25.   Šegota, S.; Ćurković, L.; Ljubas, D.; Svetlicic, V.; Houra, I.; Tomasic, N. Synthesis, characterization and photocatalytic properties of Sol-gel TiO$_2$ films. *Ceram. Int.* **2011**, *37*, 1153–1160. [CrossRef]

26.   Ćurković, L.; Ljubas, D.; Šegota, S.; Bačić, I. Photocatalytic degradation of Lissamine Green B dye by using nanostructured sol–gel TiO$_2$ films. *J. Alloys Compd.* **2014**, *604*, 309–316. [CrossRef]

27.   Švagelj, Z.; Mandić, V.; Ćurković, L.; Biošić, M.; Žmak, I.; Gaborardi, M. Titania-Coated Alumina Foam Photocatalyst for Memantine Degradation Derived by Replica Method and Sol-Gel Reaction. *Materials* **2020**, *13*, 227. [CrossRef] [PubMed]

28.   Sanchez Tobon, C.; Ljubas, D.; Mandić, V.; Panžić, I.; Matijašić, G.; Ćurković, L. Microwave-Assisted Synthesis of N/TiO$_2$ Nanoparticles for Photocatalysis under Different Irradiation Spectra. *Nanomaterials* **2022**, *12*, 1473. [CrossRef] [PubMed]

29.   Gabelica, I.; Ćurković, L.; Mandić, V.; Panžić, I.; Ljubas, D.; Zadro, K. Rapid Microwave-Assisted Synthesis of Fe$_3$O$_4$/SiO$_2$/TiO$_2$ Core-2-Layer-Shell Nanocomposite for Photocatalytic Degradation of Ciprofloxacin. *Catalysts* **2021**, *11*, 1136. [CrossRef]

30.   Ngo, H.S.; Nguyen, T.L.; Tran, N.T.; Le, H.C. Experimental Study on Kinetics and Mechanism of Ciprofloxacin Degradation in Aqueous Phase Using Ag-TiO$_2$/rGO/Halloysite Photocatalyst. *Catalysts* **2023**, *13*, 225. [CrossRef]

31.   Martins, P.; Kappert, S.; Nga Le, H.; Sebastian, V.; Kühn, K.; Alves, M.; Pereira, L.; Cuniberti, G.; Melle-Franco, M.; Lanceros-Méndez, S. Enhanced Photocatalytic Activity of Au/TiO$_2$ Nanoparticles against Ciprofloxacin. *Catalysts* **2020**, *10*, 234. [CrossRef]

32.   Hassani, A.; Khataee, A.; Karaca, S.; Fathinia, M. Heterogeneous photocatalytic ozonation of ciprofloxacin using synthesized titanium dioxide nanoparticles on a montmorillonite support: Parametric studies, mechanistic analysis and intermediates identification. *RSC Adv.* **2016**, *6*, 87569–87583. [CrossRef]

33.   Malakootian, M.; Nasiri, A.; Amiri Gharaghani, M. Photocatalytic degradation of ciprofloxacin antibiotic by TiO$_2$ nanoparticles immobilized on a glass plate. *Chem. Eng. Commun.* **2020**, *207*, 56–72. [CrossRef]

34.   Shehu Imam, S.; Adnan, R.; Mohd Kaus, N.H. Photocatalytic degradation of ciprofloxacin in aqueous media: A short review. *Toxicol. Environ. Chem.* **2018**, *100*, 518–539. [CrossRef]